Available online at www.sciencedirect.com

SCIENCE DIRECT®

Earth and Planetary Science Letters 224 (2004) 259–274

EPSL

www.elsevier.com/locate/epsl

Detection of upper mantle flow associated with the African Superplume☆

Mark D. Behn[a,*], Clinton P. Conrad[b], Paul G. Silver[a]

[a] *Department of Terrestrial Magnetism, Carnegie Institution of Washington, Washington, DC 20015, USA*
[b] *Department of Geological Sciences, University of Michigan, Ann Arbor, MI 48109, USA*

Received 2 December 2003; received in revised form 12 May 2004; accepted 17 May 2004

Abstract

A continental-scale, low seismic velocity anomaly in the mid to lower mantle beneath Africa is a robust feature of global tomographic models. Assuming the low velocities are associated with warm, less dense material, the African seismic anomaly has been ascribed to a long-lived thermal upwelling from the lower mantle. Such a large-scale upwelling should also affect the regional horizontal flow field in the upper mantle. To test this model, we compare seismic anisotropy inferred from shear-wave splitting measurements with instantaneous flow calculations that incorporate mantle density structure inferred from seismic tomography. We calculate splitting parameters at 13 ocean island stations surrounding Africa. Splitting measurements from island stations are ideal for interpreting anisotropy induced by asthenospheric flow because they lack a thick overlying lithosphere that may also contribute to the observed anisotropy. We tested for a possible lithospheric contribution by comparing the splitting measurements with the fossil spreading directions. We find that although the fossil lithospheric fabric closely matches the observed fast polarization directions at stations <500 km from a ridge axis, they are a poor fit to the data at stations located farther off-axis. Thus, we conclude that far from a ridge axis, the observed anisotropy is dominated by asthenospheric flow. To test for an active component of mantle upwelling, we considered several models with varying assumptions about the velocity at the base of the asthenosphere: that it is (1) stationary below plates moving in the no-net-rotation (NNR) or hotspot reference frames, (2) driven by plate motions at the Earth's surface, or (3) driven by a combination of plate-motion and mantle density heterogeneity inferred from either seismic tomography or the history of subduction. We find that the best-fitting flow field is generated by plate motions and density heterogeneity associated with large-scale upwelling originating in the lower mantle beneath southern Africa and is manifest as a radial pattern of flow at the base of the asthenosphere. This model provides a significantly better fit to the observed anisotropy than a model in which mantle flow is driven through a passive response to subduction. The resulting sub-asthenospheric flow field is estimated to have velocities of 0–3 cm/year, and an asthenospheric viscosity of $\sim 3{\cdot}10^{19}$ Pa·s is found to be most consistent with the regional anisotropy, geoid height, and dynamic topography.

Keywords: mantle convection; seismic anisotropy; African Superplume

☆ Supplementary data associated with this article can be found, in the online version, at doi:10.1016/j.espl.2004.05.026.

* Corresponding author. Tel.: +1-202-478-8837; fax: +1-202-478-8821.
E-mail address: behn@dtm.ciw.edu (M.D. Behn).

0012-821X/$ - see front matter © 2004 Elsevier B.V. All rights reserved.
doi:10.1016/j.epsl.2004.05.026

1. Introduction

One of the basic questions in mantle dynamics is whether mantle flow is driven solely by negative buoyancy associated with lithospheric cooling and subduction, or whether active upwelling originating in the deep mantle is a significant contribution to the global flow field. A large-scale, low seismic velocity anomaly in the mid to lower mantle beneath Africa is a robust feature of global seismic tomography models [1–3]. Assuming that low seismic velocities are associated with warm, low-density material, calculations of mantle flow predict this anomaly to be associated with a long-lived thermal upwelling from the lower mantle, often termed the "African Superplume" [4–6]. Dynamic stresses generated by this upwelling flow predict dynamic topography [7], geoid height [7,8], and surface uplift rates [8,9] that are consistent with the geologic observations. In addition, low seismic attenuation, like the low seismic velocity anomaly, has been inferred to indicate upwelling of warm material from the lower mantle beneath Africa [10].

However, these observables provide only indirect constraints on the mantle flow field, and the presence of large-scale upwelling from the lower mantle beneath southern Africa remains controversial. Based on the characteristics of global tomographic models, recent studies have suggested that chemical stratification would inhibit upwelling from the lower mantle [11]. It has also been argued that layered convection is most consistent with the Earth's geoid and dynamic topography [12–14]. If large-scale upwelling from the lower mantle is indeed present in the upper mantle beneath southern Africa, it should be detectable as a component of the horizontal flow field just below the rigid motion of the lithospheric plates. Thus, the observation of a radial pattern of flow above the African seismic anomaly would provide a direct verification that this seismic anomaly produces density-driven upwelling.

Seismic anisotropy can be used to constrain the direction of mantle flow [15,16], and therefore is ideal for testing the active-upwelling hypothesis. Anisotropy in the Earth's upper mantle is believed to be dominated by the alignment of olivine crystals in the surrounding mantle flow field [17,18]. Laboratory experiments of finite strain in olivine indicate that for simple shear, the *a*-axis of olivine is contained in the shear plane and is oriented parallel to the shear direction [19]. For shear-wave splitting the polarization direction of the fast shear wave will also be parallel to the shear direction. Assuming that the anisotropy is localized in a low-viscosity asthenosphere and is dominated by the differential motion between the lithosphere and the underlying mantle, it is possible to constrain both the direction and magnitude of the sub-asthenospheric mantle flow [20–23].

The African region is an excellent location in which to isolate the horizontal component of active upwelling in the mantle flow field due to both the close proximity of the seismic anomaly and the slow velocities of the surrounding surface plates. Several studies have found good agreement between anisotropy predicted by flow calculations that incorporate mantle density-heterogeneity and upper-mantle azimuthal anisotropy inferred from surface-wave data across the ocean basins [22,23]. However, these studies have either focused on, or have been dominated by, results in the Pacific basin, where fast plate motions dominate the observed anisotropy and make it difficult to detect non-zero velocities in the sub-asthenospheric mantle. For example, Becker et al. [22] found only a 6% improvement in global misfit for a model incorporating active upwelling compared to a model driven solely by the history of subduction. Consequently, these studies have been unable to distinguish between a mantle where flow is driven only by subduction, and a mantle that is also driven by thermal upwellings from the core–mantle boundary.

In this study, we utilize seismic anisotropy, inferred from shear-wave splitting measurements, to evaluate the active-upwelling hypothesis, and compare this hypothesis with a variety of commonly assumed alternatives regarding mantle flow beneath southern Africa. We examine models in which the velocity at the base of the asthenosphere is: (1) stationary below plates moving in the no-net-rotation (NNR) or hotspot reference frame, (2) driven by plate motion at the Earth's surface, or (3) driven by a combination of plate-motion and mantle density heterogeneity inferred from either seismic tomography or the history of subduction. We show that the best-fitting flow field is one that is driven by surface plate motions, subduction, and a large-scale upwelling originating in the lower mantle beneath southern Africa. The resulting flow field is manifest as a radial pattern of flow at the base of the asthenosphere and provides a significantly

better fit to the observed anisotropy than a mantle driven solely by the history of subduction.

2. Shear-wave splitting observations

Shear-wave splitting measurements of the fast polarization direction, ϕ, and delay time, δt, were made at 13 ocean island stations from the IRIS and GEOSCOPE networks. Splitting measurements from island stations are ideal for interpreting anisotropy induced by asthenospheric flow because they lack a thick overlying lithosphere, which often dominates the anisotropy observed at continental stations [24]. This is particularly true in southern Africa, where there is a strong correlation between the observed anisotropy and the history of continental deformation [25,26]. The island stations used in this study have good regional coverage, lying on each of the four major plates in the southern Atlantic and Indian Oceans (Fig. 1). Although estimates of seismic anisotropy derived from shear-wave splitting lack the global coverage of surface-wave data, they provide higher lateral resolution and are not biased by trade-offs with isotropic lateral heterogeneity. Splitting

Table 1
Shear-wave splitting parameters with 2σ errors at island stations

Station	No. of events	ϕ (°)	δt (s)
AIS	7	46 ± 11	0.63 ± 0.47
ASCN	20	81 ± 11	0.86 ± 0.16
CMLA	20	-61 ± 7	0.60 ± 0.17
COCO	4	59 ± 17	0.69 ± 0.47
CRZF	12	-32 ± 15	0.55 ± 0.31
HOPE	9	50 ± 5	0.76 ± 0.15
MSEY	35	32 ± 3	1.02 ± 0.11
PAF	11	-77 ± 10	1.34 ± 0.36
PALK	12	26 ± 2	1.72 ± 0.35
RER	11	-81 ± 8	0.77 ± 0.16
SACV	7	52 ± 11	1.02 ± 0.58
SHEL	8	59 ± 6	0.83 ± 0.26
TBT	21	17 ± 5	0.92 ± 0.43

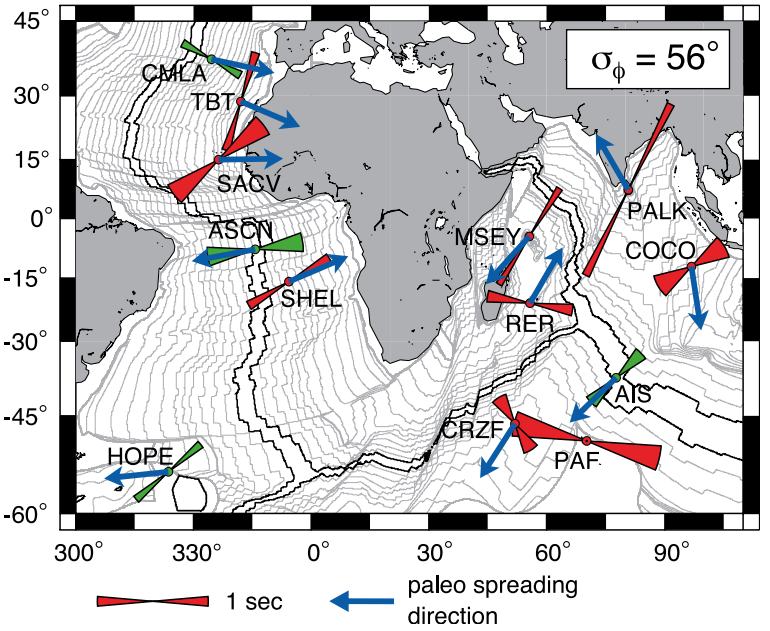

Fig. 1. Comparison of splitting observations to fossil spreading directions determined from seafloor magnetic anomalies. Fossil spreading directions are shown by blue vectors pointing toward older seafloor. No fossil spreading direction is reported at station PAF due to the lack of well-constrained seafloor magnetic anomalies. Observed splitting parameters are illustrated by red (>500 km from a plate boundary) and green (<500 km from a plate boundary) symbols, with symbol length representing the delay time and width showing the 2σ-error in the fast-polarization direction. Fast polarization directions closely follow the fossil lithospheric fabric for stations <500 km from the ridge axis, however, lithospheric fabric is a poor fit to the data at stations far from a ridge.

parameters were calculated for each station from SKS and SKKS phases by stacking a suite of earthquakes [18,27,28]. This method is advantageous because it provides high-quality estimates of receiver splitting at island stations where individual measurements tend to be noisy and of poor quality.

The calculated splitting parameters are given in Table 1 and shown in Fig. 1. A list of events and the individual phases used in each station stack are provided in Tables S1 and S2, respectively (see the online version of this paper). In general, our observations are consistent with previous splitting measurements at island stations surrounding Africa. In the Atlantic, the calculated splitting parameters at stations TBT, ASCN, SHEL, and HOPE are in good agreement with previous estimates from individual events [29,30], as is station MSEY in the Indian Ocean [29]. We note that an earlier study [31] looking at data collected before 1996 failed to detect anisotropy at stations PAF, RER, CRZF and AIS in the Indian Ocean. We interpret our ability to obtain high-quality splitting estimates at these stations to reflect both the incorporation of additional data as well as the importance of stacking events in high noise environments. Station RER provides a good example of the utility of stacking in order to obtain robust splitting parameters. RER is particularly significant because of its importance in distinguishing between the competing models

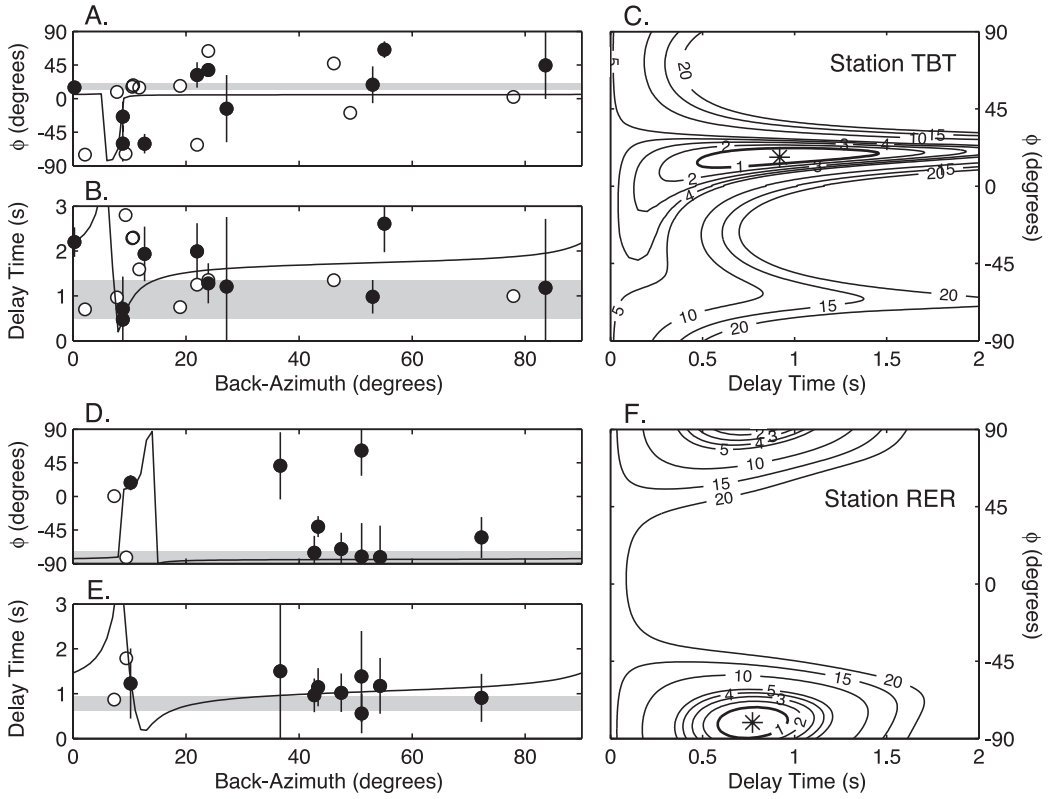

Fig. 2. Splitting parameters (A) ϕ and (B) δt as a function of event back-azimuth (modulo 90°) for station TBT. Black symbols indicate splitting parameters calculated for non-null events, open symbols show nulls. Grey bars illustrate best-fit splitting parameters calculated from the stacking method of Wolfe and Silver [27]. The two-layer inversion at station TBT (see text for details) resulted in a model with: $\phi_{lith} = 113°$ (fixed), $\delta t_{lith} = 0.2$ s, $\phi_{asth} = 8°$, $\delta t_{asth} = 1.9$ s. Solid line shows predicted apparent splitting parameters for the two-layer inversion. (C) Contour plot of the minimum eigenvalue of the corrected matrix of particle motion calculated by stacking all events at station TBT. (D–F) Station RER. The two-layer inversion at station RER resulted in a model with: $\phi_{lith} = 30°$ (fixed), $\delta t_{lith} = 0.2$ s, $\phi_{asth} = 102°$, $\delta t_{asth} = 1.2$ s. The lack of strong dependence of the splitting parameters on event backazimuth at both stations suggests that the observed anisotropy can be explained simply by a one-layer model.

for mantle flow presented later in this study. Fig. 2 shows the splitting parameters calculated from individual events as a function of back azimuth as well as the stacked solution for station RER. Both the null and non-null measurements are compatible with the stacked solution. Similar results at stations PAF, CRZF and AIS allow us to conclude that the splitting parameters presented here provide a good estimate for the anisotropy beneath these stations.

3. Comparison to fossil seafloor fabric

Numerical models of mantle flow at mid-ocean spreading centers [21,22,32] and the orientation of olivine aggregates in ophiolites [33,34] indicate that the fast polarization direction in the lithosphere is parallel to the spreading direction. Therefore, we tested for a possible lithospheric contribution to the observed anisotropy by comparing the orientation of ϕ to the fossil spreading direction inferred from seafloor magnetic anomalies (Fig. 1). The model fit is quantified by the RMS angular difference, σ_ϕ, between the predicted and observed orientation of ϕ. For a perfect model, σ_ϕ should be smaller than or about 5°, the standard error in ϕ for our splitting measurements. We include only the orientation of ϕ in our analysis. Delay times were neglected due to the difficulties in distinguishing between the magnitude of the anisotropic fabric and the thickness of the anisotropic layer. We find that for stations located <500 km from a mid-ocean ridge axis (CMLA, ASCN, AIS), the fast polarization directions closely follow the fossil lithospheric fabric ($\sigma_\phi = 10°$), indicating that corner flow associated with spreading dominates the near-ridge mantle flow field. However, for stations >500 km from a ridge axis, lithospheric fabric is a poor fit to the data ($\sigma_\phi = 56°$).

To further investigate the presence of a separate component of lithospheric anisotropy, we examined the splitting parameters as a function of event backazimuth [35,36]. If two layers, such as a lithosphere and asthenosphere, contribute to the net anisotropy separately, both ϕ and δt will vary with backazimuth. However, such variations are not observed at any of the stations. We further performed a formal inversion for a two-layer model, assuming the fast-axis direction in the upper layer was equal to the fossil spreading direction. Fig. 2 shows the results of this inversion for stations TBT and RER, where the observed fast axis direction is more than 60° from the fossil spreading direction. In both cases, the inversion finds only a small component of lithospheric anisotropy ($\delta t_{\mathrm{lith}} \leq 0.2$ s). Thus, we conclude that for the stations in this study, the observed anisotropy is dominated by asthenospheric flow. For stations near the ridge axis, this flow is dominated by corner flow associated with ridge spreading.

4. Models for sub-asthenospheric mantle flow

We next consider a series of models for mantle flow, each of which predicts a distinct velocity field at the base of the asthenosphere and a corresponding value of ϕ. Specifically, we test models in which flow is (1) stationary below plates moving in the no-net-rotation (NNR) or hotspot reference frames, (2) driven by plate motions at the Earth's surface, (3) driven by a combination of plate motions and the negative buoyancy of slabs or (4) driven by plate motions and mantle density heterogeneity inferred from seismic tomography. This last case includes the possible influence of active upwellings. Following Zhang and Karato [19], we choose the direction of maximum shear at the center of the asthenosphere as a proxy for the predicted orientation of the olivine *a*-axis in our flow calculations. The maximum shear direction is computed from the horizontal projection of the largest extensional eigenaxis of the strain-rate tensor [23]. We choose this proxy due to its simplicity and the assumption that the olivine *a*-axis will align rapidly with the local strain-rate tensor. However, in regions where the strain-rate tensor changes rapidly along the flow path, it may be more appropriate to estimate olivine fabric by tracking finite strain (e.g., [15,22,32,37]).

Because measurements of shear-wave splitting are sensitive to the depth-integrated anisotropy, it is important to quantify the depth dependence of the direction of maximum shear. For the models presented in this study, we find that the variation in the maximum shear direction throughout the asthenosphere is small, with an average standard deviation of 10° relative to the shear direction at the center of the asthenosphere. In addition, the splitting parame-

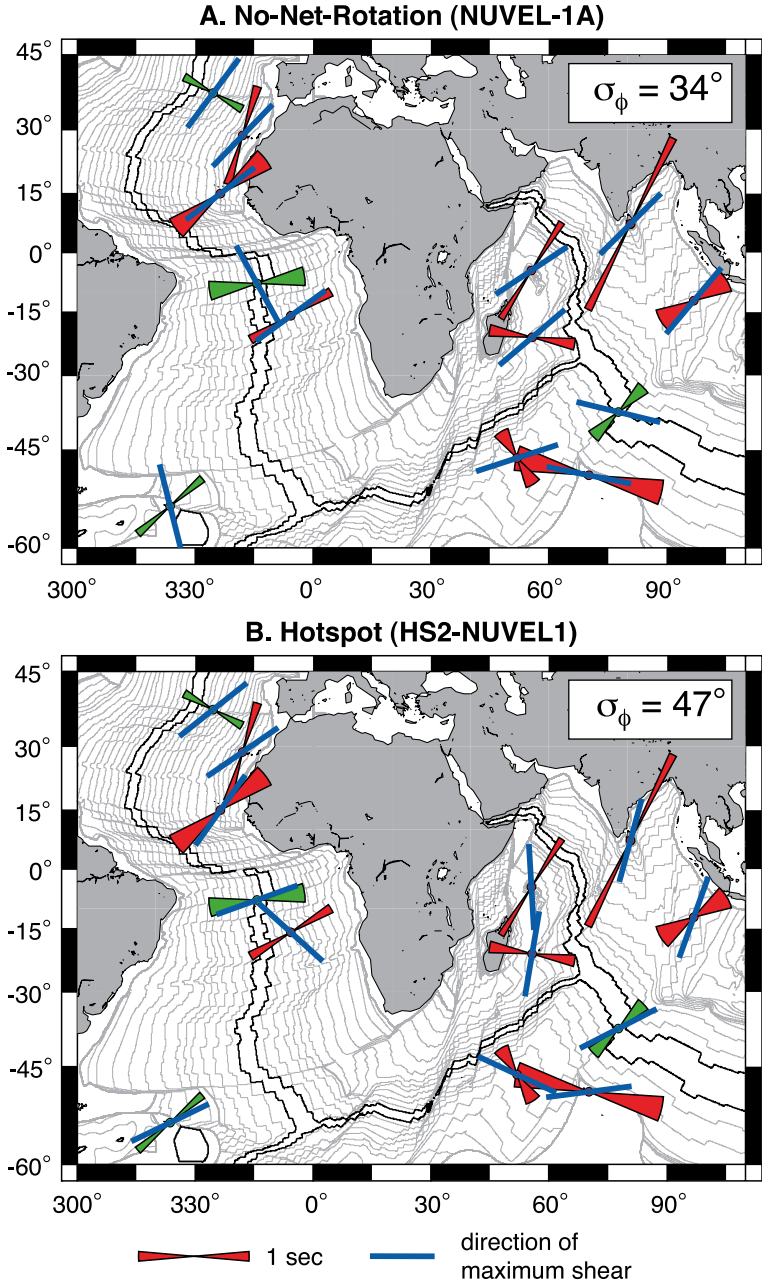

Fig. 3. Comparison of splitting observations to plate motions in the (A) no-net-rotation (NUVEL-1A) [40] and (B) hotspot (HS2-NUVEL1) [41] reference frame. Blue bars show direction of shear, which is oriented parallel to plate motion. Observed splitting parameters are illustrated by the red and green symbols, as in Fig. 1. In the case of plate motion over a stationary asthenosphere, the direction of shear and hence ϕ will be oriented parallel to plate motion. The anisotropy predicted for a stationary asthenosphere in both the NNR or the hotspot reference frames does not fit the observed splitting data.

ters had little or no dependence on event back-azimuth, indicating a lack of vertical heterogeneity in the anisotropy. Therefore, we conclude that the splitting observations can be interpreted within the context of a single homogeneous anisotropic layer. Laboratory experiments that relate anisotropy to finite strain have shown that elevated water content (>400 ppm H/Si) and stress (>150 MPa) result in deformation mechanisms that significantly complicate the relationship between flow and the orientation of seismic anisotropy [38]. However, we assume that the source of the observed anisotropy is isolated to the asthenosphere, where water content is likely low [39] and the calculated stresses associated with mantle flow are on the order of 1–10 MPa. Under these conditions, the observed fast polarization direction should align with the orientation of maximum shear.

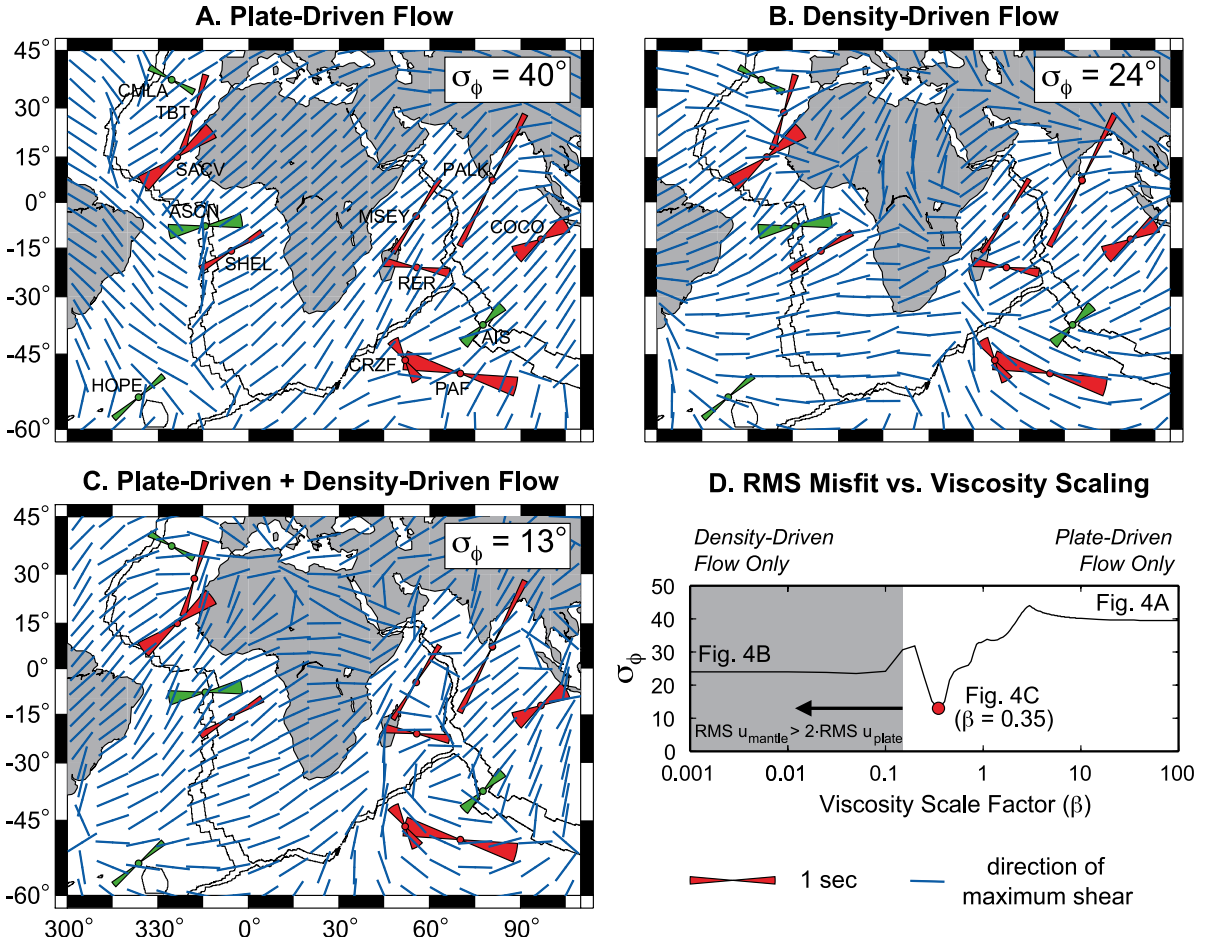

Fig. 4. Horizontal projection of the shear direction calculated from the *reference* viscosity structure for (A) plate-driven flow, (B) density-driven flow, and (C) plate-driven + density-driven flow ($\beta = 0.35$). Observed splitting parameters are illustrated by the red (>500 km from a plate boundary) and green (<500 km from a plate boundary) symbols. Symbol length represents delay time and width shows 2σ-error in the fast-polarization direction. (D) RMS angular difference, σ_ϕ, between the orientation of the predicted anisotropy and the observed fast-polarization directions as a function of the viscosity scale factor, β. The grey region illustrates viscosity structures in which the RMS mantle velocity at the base of the asthenosphere is a factor of two or more larger than the RMS plate velocity across the study area. For large-scale factors, the magnitude of the density-driven component of flow will be small and the plate-driven component of flow will dominate. In contrast, for small values of β, the density-driven component of flow will dominate. A scale factor of $\beta = 0.35$ results in the best-fitting flow field characterized by $\sigma_\phi = 13°$.

4.1. Stationary sub-asthenospheric mantle

For the case of plate motion over a stationary sub-asthenospheric mantle, the direction of shear and hence ϕ will be parallel to plate motion. Therefore, to test this model, we compared the observed fast polarization directions directly to plate motion vectors in the NNR [40] and hotspot [41] reference frames (Fig. 3). We find that neither reference frame is able to adequately explain all the data (NNR $\sigma_\phi = 46°$; Hotspot $\sigma_\phi = 44°$). For plate motions in the NNR frame, σ_ϕ is improved to 34° by eliminating stations located <500 km from a plate boundary (CMLA, ASCN, AIS, HOPE), where we have shown that flow associated with ridge spreading may dominate the flow field. However, systematic misfit at stations in the Indian and central Atlantic Oceans suggests that the mantle is not stationary and that a component of sub-asthenospheric flow must contribute to the observed anisotropy. In the case of the hotspot reference frame, the removal of the plate boundary stations results in a larger misfit ($\sigma_\phi = 47°$) than when all the stations are

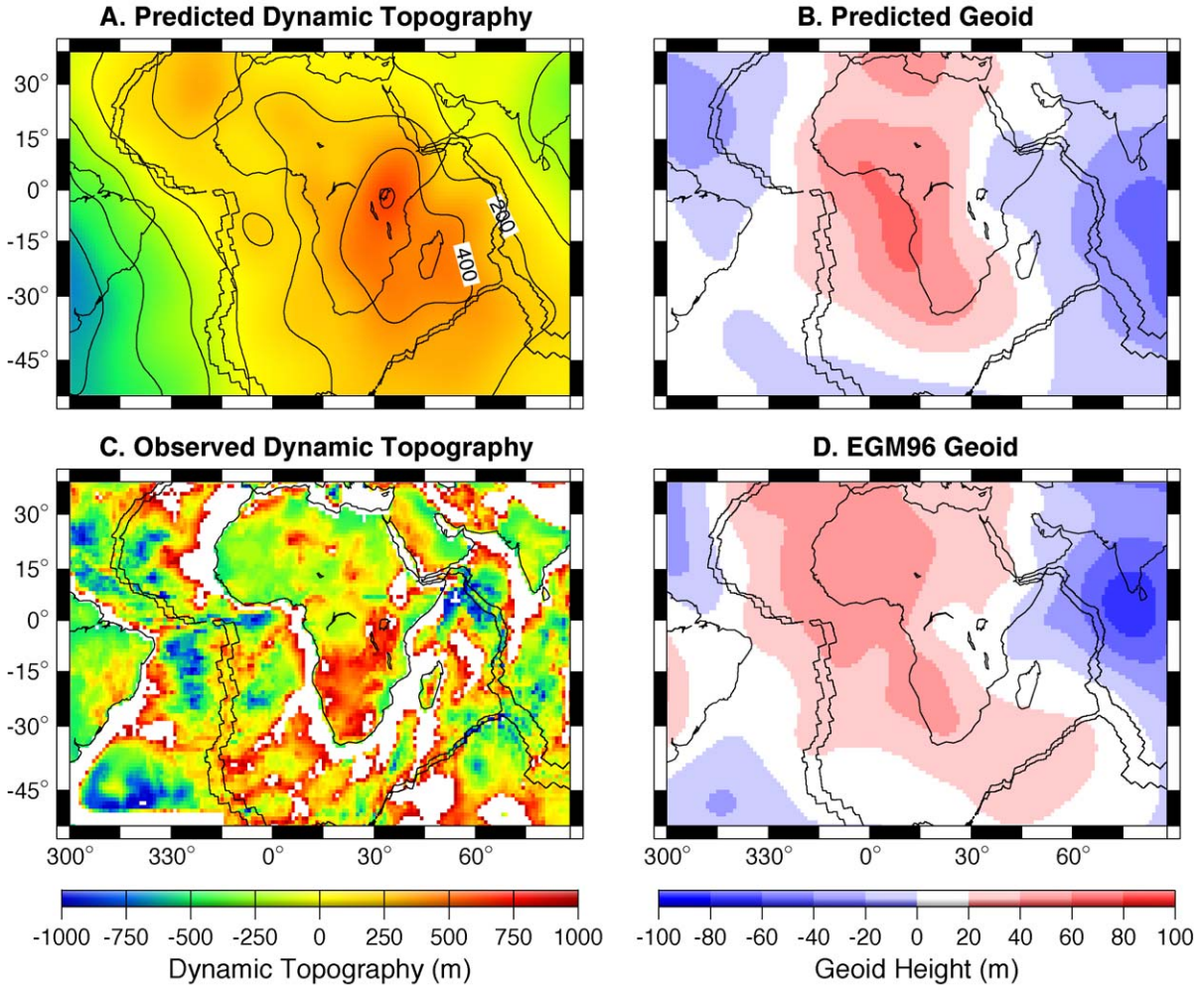

Fig. 5. (A) Dynamic topography calculated following Lithgow-Bertelloni and Silver [7] and (B) predicted geoid calculated for the *reference* viscosity structure assuming a velocity-to-density scaling of 0.15 g/cm^3/km/s. (C) Estimated dynamic topography [55]. Continental shelves and areas with elevations greater than 1000 m are shown in white. Anomalous topography in these regions is likely related to local lithospheric structure. (D) Observed EGM96 geoid [56], expressed relative to the Earth's hydrostatic ellipsoid [57].

included. Thus, a stationary asthenosphere coupled with plate motions in either reference frame cannot explain the observed anisotropy.

4.2. Plate-driven flow

To determine whether mantle flow driven by plate motions is consistent with the observed anisotropy, we calculated the instantaneous mantle flow field [42] after imposing global plate motions for 13 plates in the NNR reference frame. We assume a laterally homogeneous, but radially varying *reference* viscosity structure that is divided into four layers [43]: lithosphere (0–100 km, $\eta_{\mathrm{lith}} = 30 \times 10^{21}$ Pa·s), asthenosphere (100–300 km, $\eta_{\mathrm{asth}} = 0.1 \times 10^{21}$ Pa·s), upper mantle (300–670 km, $\eta_{\mathrm{um}} = 1 \times 10^{21}$ Pa·s), and lower mantle (670–2800 km, $\eta_{\mathrm{lm}} = 50 \times 10^{21}$ Pa·s). Shear associated with the resulting flow field is concentrated in the low-viscosity asthenosphere; thus, we compare the observed fast polarization directions to the orientation of maximum shear calculated at the center of the asthenosphere (Fig. 4A). After eliminating stations <500 km from a plate boundary, we find the predicted anisotropy for plate-driven flow is also a poor fit to the observed splitting measurements ($\sigma_\phi = 40°$). Moreover, varying the viscosity or thickness of the lithospheric or asthenospheric layers relative to the *reference* viscosity structure did not significantly improve the fit to the splitting data.

4.3. Plate-driven+density-driven flow: with active upwelling

We next calculated mantle flow associated with internal density variations derived from the S20RTS global tomography model [3]. A constant S-wave velocity-to-density scaling of 0.15 g/cm^3/km/s was assumed for all depths below 325 km. Following Lithgow-Bertelloni and Silver [7], we ignore density variations above 325 km as the seismically fast velocity anomalies associated with continental roots have been shown to be neutrally buoyant [44]. A depth of 325 km was chosen to correspond with the base of the African craton as imaged by local P- and S-wave tomography [45]. However, sensitivity tests using shallower cutoff depths (e.g., 100, 175, and 250 km) show that with the exception of station MSEY,

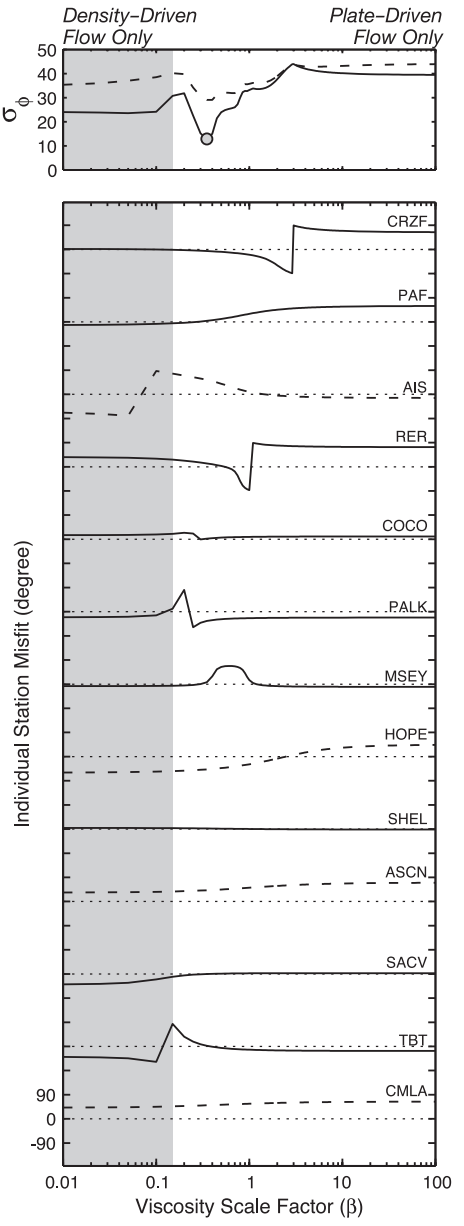

Fig. 6. (Top) RMS angular difference, σ_ϕ, as a function of the viscosity scale factor, β, calculated for all stations assuming density heterogeneity derived from the S20RTS tomography model [3]. (Bottom) Angular misfit as a function of β at each station. Dashed lines denote stations located <500 km from an active plate boundary. The grey region illustrates viscosity structures in which the RMS mantle velocity at the base of the asthenosphere is a factor of two or more larger than the RMS plate velocity across the study area. Note that the sharp zero crossings in the station misfit traces are caused by the 90°-periodicity of the misfit.

the predicted shear direction is relatively insensitive to the depth cutoff used. The velocity-to-density scaling of 0.15 g/cm^3/km/s is consistent with laboratory data [46] and results in dynamic topography that matches geologic observations (Fig. 5). To isolate the density-driven flow field from flow associated with known surface plate motions, we calculate flow in the absence of plate motions. Upwelling associated with the observed low-velocity anomaly in the mid to lower mantle generates a radial pattern of flow at the base of the asthenosphere around southern Africa. The resulting directions of maximum shear have a similar radial pattern (Fig. 4B), resulting in a value of $\sigma_\phi = 24°$ for stations located >500 km from a plate boundary. Furthermore, the density-driven flow field provides a significantly better fit to stations RER, PAF, CRZF, TBT, and CMLA than does plate-driven flow (see Fig. 4A and B).

The actual mantle flow field will be a combination of both plate-driven and density-driven flow. Ultimately, plate motions are driven by density heterogeneity in the mantle, but a full description of the coupling between mantle flow and plate motions has not been achieved in numerical models [47]. This problem is particularly pronounced for plates, such as the African plate, that are not directly attached to subducting slabs. Because seismic anisotropy constrains the relative motions between the plates and the underlying mantle, we must use the correct surface plate motions in order to compare the predicted anisotropy with the splitting observations. By adding the density-driven flow field to the plate-driven field,

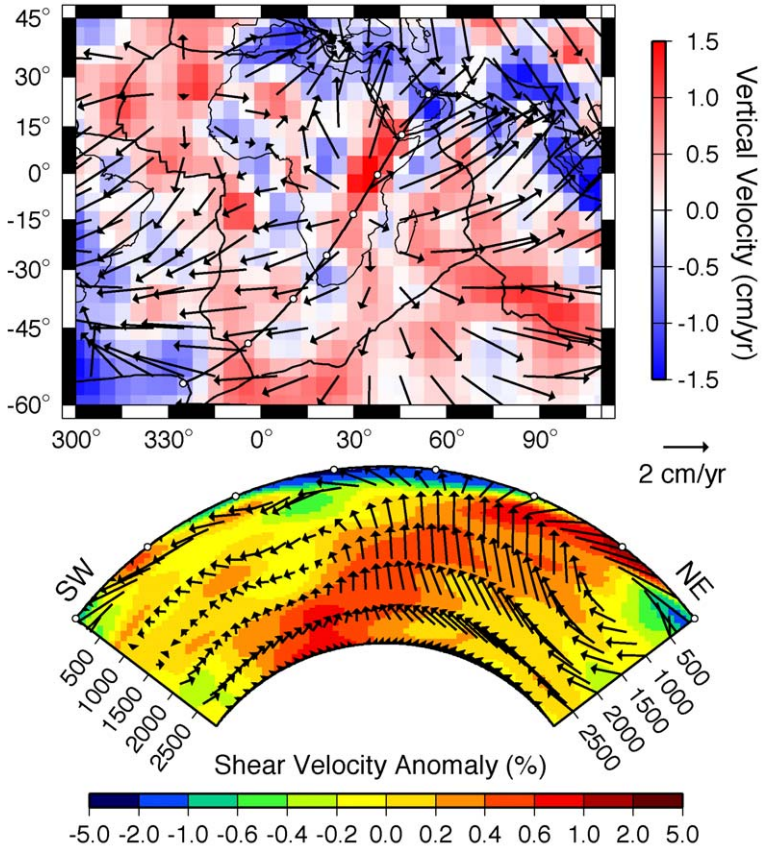

Fig. 7. (Top) Map-view of the plate-driven + density-driven flow field at the base of the asthenosphere (depth = 300 km, $\beta = 0.35$). Arrows illustrate horizontal flow and colors depict vertical velocities. Thick black line shows location of cross-section in lower panel. (Bottom) Cross-section through the S20RTS tomography model [3]. Arrows show predicted upwelling flow associated with the low-velocity anomaly in the mid to lower mantle. The upwelling is manifest as a radial flow field at the base of the asthenosphere.

we create a combined flow model that includes the proper surface plate motions. However, this model does not include balanced torques on each plate. Instead, we must assume, as others have done [22], that unmodeled complexity, such as plate-plate or plate-slab interactions [47], accounts for the differences between the driving and resisting forces on plates.

For plate-driven flow, the strain-rates in the mantle are determined by the imposed surface plate velocities and are independent of the absolute mantle viscosity. In contrast, for density-driven flow, the imposed density-heterogeneity field results in strain-rates whose magnitudes are inversely proportional to the absolute mantle viscosity. Thus, the importance of density-driven flow in the combined flow field depends on the absolute mantle viscosity. Therefore, by multiplying the *reference* viscosity structure by a constant scale factor, β, and summing the resulting plate-driven and density-driven components of flow, we can solve for the absolute mantle viscosity structure that best fits the observed splitting data.

A β-value of 0.35 results in the best-fitting mantle flow field—characterized by $\sigma_\phi = 13°$ for stations located >500 km from a plate boundary (Fig. 4C and D). The total misfit as well as the individual station misfits are shown as a function of the viscosity scale factor, β, in Fig. 6. The best-fit viscosity scaling implies an asthenospheric viscosity of $\sim 3.5 \cdot 10^{19}$ Pa·s, approximately one order of magnitude higher than estimates of upper mantle viscosity inferred from post-seismic relaxation [48]. The higher viscosity calculated in this study can be attributed to averaging over the entire asthenosphere, in contrast to post-seismic relaxation studies, which are most sensitive to the viscosity of the uppermost asthenosphere. We also find that the "average" upper mantle viscosity calculated in this study is similar to that inferred from post-glacial rebound [49]. Because the predicted anisotropy is primarily determined by the differential velocity between the top and bottom of the asthenosphere, we also directly constrain the magnitude of the mantle velocities at the base of the asthenosphere (Fig. 7). For the best-fitting flow field, we find that the RMS mantle velocity at the base of the asthenosphere is 2.6 cm/year, similar to the RMS plate velocity of 2.7 cm/year across the study area. We note that this estimate is insensitive to the velocity-to-density scaling or absolute viscosity used.

To evaluate the relative importance of density-driven flow originating in the middle versus the lower mantle, we calculate a series of models ignoring all density perturbations (i.e., velocity-to-density scaling = 0 g/cm^3/km/s) below a given depth. In each case the best-fitting flow field is determined by inverting for a viscosity scale factor, β, as described above. We find that flow driven by density heterogeneity in the depth range from 1500 to 2500 km is required to explain the observed anisotropy (Fig. 8). This observation provides strong evidence that upwelling from the lower mantle beneath southern Africa is expressed in the upper mantle flow field. Fig. 8 also shows that flow driven by density perturbations in the lowermost 300 km of the mantle has little effect on the model fit. Several recent studies have suggested that chemical rather than thermal heterogeneities may dominate the relationship between seismic velocity and density in the lowermost mantle [45,50,51]. Specifically, these studies predict that velocity perturbations associated with chemical anomalies are either poorly or nega-

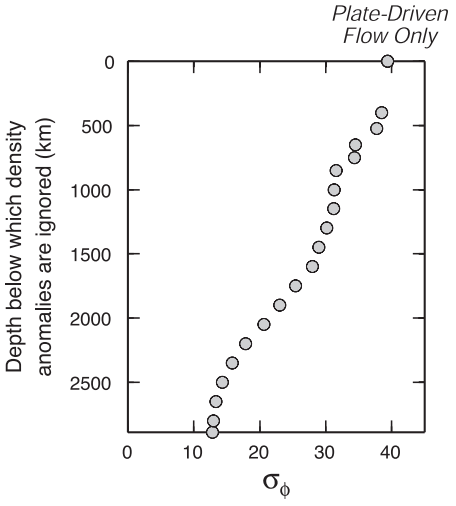

Fig. 8. RMS angular difference, σ_ϕ, versus the depth below which mantle density structure does not contribute to driving flow. The angular misfit is calculated after inverting for the best-fitting viscosity scale factor, β. Note that flow driven by density anomalies residing in the lowermost 300 km of the mantle are not critical to fit the splitting observations. However, ignoring density structure in the region between 1500 and 2500 km significantly degrades the fit to the observed anisotropy.

tively correlated to density. The lack of correlation between the model fit and the density structure in lowermost mantle (Fig. 8) is consistent with the inference that velocity anomalies are not tied to thermal structure in this region. However, our data alone provide no conclusive test of this hypothesis.

The Earth's geoid provides an additional constraint on the global pattern of mantle convection (e.g., [4]). Thus, it is important to insure that the flow field that best fits the anisotropy is also consistent with the observed geoid. We assume a free-slip surface boundary condition, which has been shown to produce a good fit to the global geoid [52] and allows for lateral motion of the surface plates. Using the *reference* viscosity structure and a velocity-to-density scaling of 0.15 g/cm^3/km/s, the predicted geoid for the S20RTS model results in a good fit to the observed geoid within the study area (Fig. 5) and a global variance reduction of 0.57. This global variance reduction is comparable to the best-fitting unlayered models of previous studies [52].

4.4. Plate-driven+density-driven flow: without active upwelling

The previous calculations assume that the flow field beneath southern Africa is driven by active upwelling associated with a thermal anomaly in the

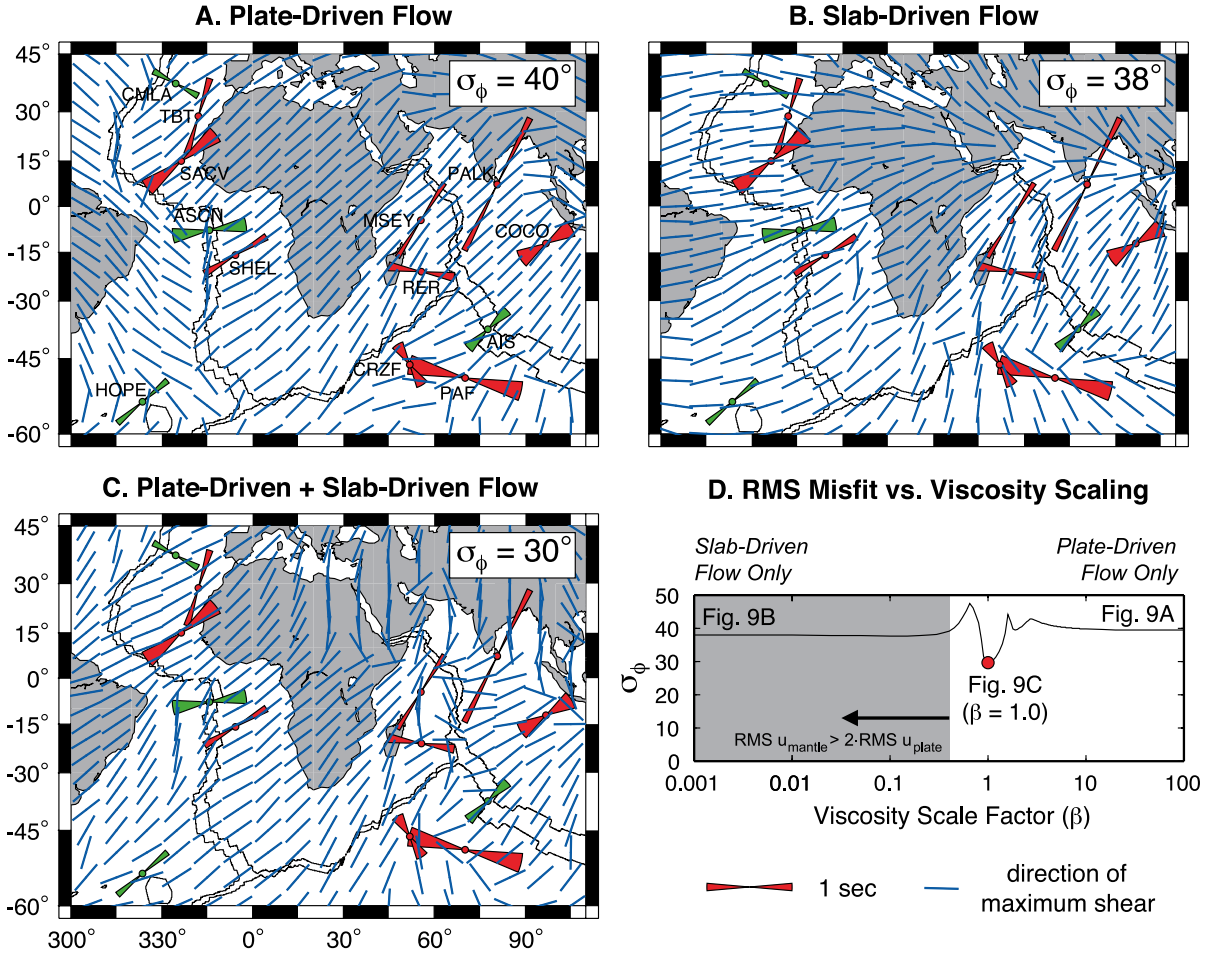

Fig. 9. Similar to Fig. 4, but for slab-driven flow calculated from mantle density heterogeneity based on the history of subduction over the past 200 My [53,54]. In this case, a scale factor of $\beta = 1.0$ results in the best-fitting flow field ($\sigma_\phi = 30°$). Note that flow associated with the history of subduction is a poorer fit to the observed anisotropy than is flow driven by active upwelling beneath southern Africa.

mid to lower mantle. However, broad-scale return flow in response to subduction in the Pacific basin will tend to generate passive upwelling beneath the African region [7] as well as beneath the Pacific basin. To determine whether mantle flow associated with active or passive upwelling is a better fit to the splitting data, we calculated the flow field associated with a model for mantle density heterogeneity based on the history of subduction over the past 200 My [53,54]. After inverting for the best-fit asthenospheric viscosity in the manner described above, we find that the combined plate-driven + slab-driven flow field at the base of the asthenosphere (Fig. 9C) is less radial than that associated with active upwelling (Fig. 4C). The resulting flow field is a poorer fit to the observed anisotropy, with a misfit ($\sigma_\phi = 30°$) that is more than twice that for the tomography-based model (Fig. 10). Thus, an active, rather than passive, upwelling appears to be required by the data. This result is consistent with the previous observation that passive flow driven by subduction cannot produce the dynamic topography observed in the African superswell region [7].

To further investigate whether active upwelling beneath southern Africa is necessary to explain the splitting observations, we calculate flow associated with density heterogeneity derived from the S20RTS tomography model excluding density variations beneath the African plate. This removes nearly all the seismically slow material that drives upwelling beneath Africa, but retains the seismically fast anomalies associated with the major subduction zones [3]. Inverting for the best-fit asthenospheric viscosity, we find the resulting flow field to have a misfit of $\sigma_\phi = 26°$, again a factor of ~ 2 worse than a model that includes the large-scale low seismic velocity anomaly beneath Africa. Thus, we conclude that active upwelling driven by density heterogeneity in the lower mantle is necessary to explain the anisotropy observed around southern Africa.

5. Discussion/conclusions

This study provides the most direct evidence to date that a horizontal component of flow associated with active upwelling from the deep mantle is present in the upper mantle flow field. Incorporating density heterogeneity from seismic tomography results in greater than 80% variance reduction between the predicted and observed anisotropy relative to a model that includes only the history of subduction. In con-

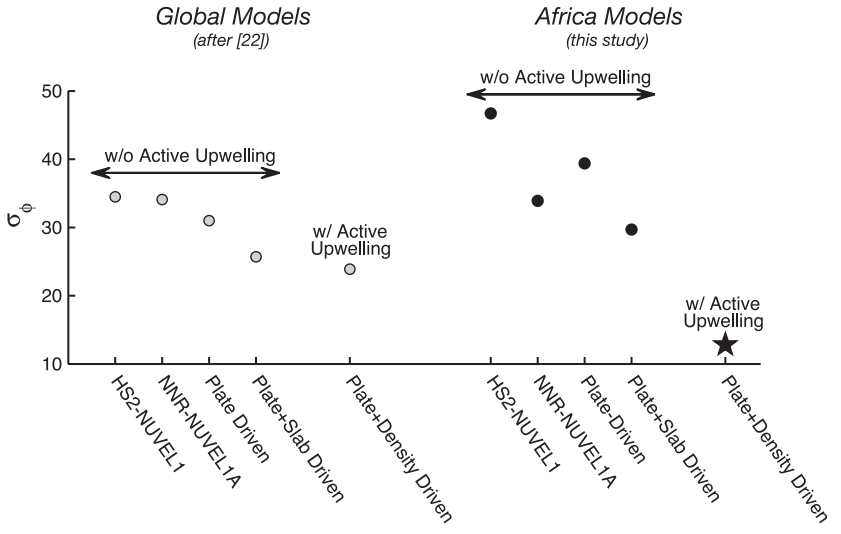

Fig. 10. RMS angular difference, σ_ϕ, between the orientation of the predicted anisotropy and the observed fast-polarization directions for different models of sub-asthenospheric flow. Note that global studies (e.g., [22]) have difficulty distinguishing between active and passive models for mantle flow. However, in the African region, the best-fitting model for sub-asthenospheric flow requires a component of active upwelling beneath southern Africa.

trast, global studies that compared anisotropy predicted from mantle flow to anisotropy inferred from surface-wave data have found that including tomography-based density structure results in only a slight improvement over slab-driven models (e.g., [22]) (see Fig. 10). We hypothesize that this difference is due to the reduced sensitivity of global studies to the sub-asthenospheric velocity field induced by active upwelling. Instead, these global assessments are likely dominated by data from the Pacific Ocean basin, where fast moving plates mask the underlying density-driven velocity field. The slower plate velocities in the African region result in anisotropy that is more sensitive to the mantle velocity field at the base of the asthenosphere, and, coupled with the close proximity of the African seismic anomaly, provide a superior test for a horizontal component of flow associated with active upwelling.

Our results argue against convection models in which chemical stratification blocks all flow between the upper and lower mantle (see Fig. 8). However, hybrid models in which upwelling flow is partially blocked in the mid-mantle (e.g., [13,14]) cannot be excluded and future modeling studies are necessary to test these scenarios. Furthermore, although the active-upwelling model provides the best fit to the observed anisotropy, the predicted misfit ($\sigma_\phi = 13°$) remains larger than the standard error in the splitting measurements. We hypothesize that the remaining misfit is associated with local lithospheric structure at individual stations and limitations in our modeling approach, which does not include the effects of lateral variations in viscosity. Finally, the relationship observed between ϕ and the fossil lithospheric fabric shows an intriguing dependence on distance from an active spreading center. Specifically, our data suggest that there is a transition between regions in which anisotropy is dominated by corner flow associated with spreading, and off-axis regions where anisotropy is dominated by the global mantle flow field. Future seismic experiments are necessary to investigate this transition and its implications for local mantle flow near mid-ocean ridges.

For the past few decades, plate motion, geoid height, and dynamic topography have been the three principal constraints on global models of mantle circulation. However, the plate motion constraint permits a wide range of mantle flow models, and geoid height and dynamic topography are independent of the absolute mantle viscosity. By incorporating seismic anisotropy as a direct constraint on the differential velocity between plate motion and sub-asthenospheric mantle flow, it is possible to estimate both the absolute mantle viscosity and the absolute velocity of mantle flow. The results of this study strongly support a model in which flow associated with active upwelling originating in the lower mantle makes a significant contribution to the sub-asthenospheric flow field. We observe this large-scale upwelling to be manifest as a radial pattern of flow in the upper mantle surrounding southern Africa, with magnitudes comparable to regional plate velocities. Using seismic anisotropy to directly estimate mantle flow, it will soon be possible to answer other long-standing questions regarding the relationship between plate tectonics and mantle convection.

Acknowledgements

We thank Derek Schutt for his assistance with the shear-wave splitting analysis. This study greatly benefited from discussions with Guilhem Barruol, C. Lithgow-Bertelloni, Roger Buck, Kevin Burke and Greg Hirth as well as thoughtful reviews by Thorsten Becker, Caroline Beghein, and an anonymous reviewer. Financial support was provided by a Carnegie Postdoctoral Fellowship (Behn), the David and Lucille Packard Foundation (Conrad), and NSF Grant 0215616 (Silver). ***[RV]***

References

[1] A.M. Dziewonski, Mapping the lower mantle: determination of lateral heterogeneity in P velocity up to degree and order 6, J. Geophys. Res. 89 (1984) 5929–5952.
[2] S.P. Grand, R.D. van der Hilst, S. Widiyantoro, Global seismic tomography: a snapshot of convection in the earth, GSA Today 7 (1997) 1–7.
[3] J. Ritsema, H.J. van Heijst, J.H. Woodhouse, Complex shear wave velocity structure imaged beneath Africa and Iceland, Science 286 (1999) 1925–1928.
[4] B.H. Hager, R.W. Clayton, M.A. Richards, R.P. Comer, A.M. Dziewonski, Lower mantle heterogeneity, dynamic topography and the geoid, Nature 313 (1985) 541–545.
[5] A.M. Forte, J.X. Mitrovica, Deep-mantle high-viscosity flow

and thermochemical structure inferred from seismic and geodynamic data, Nature 410 (2001) 1049–1056.
[6] A.M. Forte, J.X. Mitrovica, A. Espesset, Geodynamic and seismic constraints on the thermochemical structure and dynamics of convection in the deep mantle, Philos. Trans. R. Soc. Lond. A. 360 (2002) 2521–2543.
[7] C. Lithgow-Bertelloni, P.G. Silver, Dynamic topography, plate driving forces and the Africa superswell, Nature 395 (1998) 269–272.
[8] M. Gurnis, J.X. Mitrovica, J. Ritsema, H.-J. van Heijst, Constraining mantle density structure using geological evidence of surface uplift rates: the case of the African Superplume, Geochem. Geophys. Geosys. 1 (2000) (10.1029/1999GC000035).
[9] C.P. Conrad, M. Gurnis, Seismic tomography, surface uplift, and the breakup of Gondwanaland: integrating mantle convection backwards in time, Geochem. Geophys. Geosys. 4 (2003) (10.1029/2001GC000299).
[10] B. Romanowicz, Y. Gung, Superplumes from the core–mantle boundary to the lithosphere: implications for heat flux, Science 296 (2002) 513–516.
[11] L.H. Kellogg, B.H. Hager, R.D. van der Hilst, Compositional stratification in the deep mantle, Science 283 (1999) 1881–1884.
[12] L. Wen, D.L. Anderson, Layered mantle convection: a model for geoid and topography, Earth Planet. Sci. Lett. 146 (1997) 367–377.
[13] O. Cadek, L. Fleitout, A global geoid model with imposed plate velocities and partial layering, J. Geophys. Res. 104 (1999) 29055–29075.
[14] O. Cadek, L. Fleitout, Effect of lateral viscosity variations in the top 300 km on the geoid and dynamic topography, Geophys. J. Int. 152 (2003) 566–580.
[15] D.P. McKenzie, Finite deformation during fluid flow, Geophys. J. R. Astron. Soc. 58 (1979) 689–715.
[16] N.M. Ribe, Seismic anisotropy and mantle flow, J. Geophys. Res. 97 (1989) 4213–4223.
[17] A. Nicolas, N.I. Christensen, Formation of anisotropy in upper mantle peridotites, in: K. Fuchs, C. Froidevaux (Eds.), Composition, Structure and Dynamics of the Lithosphere–Asthenosphere System, Geodynamics, vol. 16, AGU, Washington, DC, 1987, pp. 111–123.
[18] P.G. Silver, W.W. Chan, Shear wave splitting and subcontinental mantle deformation, J. Geophys. Res. 96 (1991) 16429–16454.
[19] S. Zhang, S. Karato, Lattice preferred orientation of olivine aggregates deformed in simple shear, Nature 375 (1995) 774–777.
[20] P.G. Silver, W.E. Holt, The mantle flow field beneath western North America, Science 295 (2002) 1054–1057.
[21] D.R. Toomey, W.S.D. Wilcock, J.A. Conder, D.W. Forsyth, J.D. Blundy, E.M. Parmentier, W.C. Hammond, Asymmetric mantle dynamics in the MELT region of the east pacific rise, Earth Planet. Sci. Lett. 200 (2002) 287–295.
[22] T.W. Becker, J.B. Kellogg, G. Ekström, R.J. O'Connell, Comparison of azimuthal seismic anisotropy from surface waves and finite-strain from global mantle-circulation models, Geophys. J. Int. 155 (2003) 696–714.
[23] C. Gaboret, A.M. Forte, J.-P. Montagner, The unique dynamics of the Pacific Hemisphere mantle and its signature on seismic anisotropy, Earth Planet. Sci. Lett. 208 (2003) 219–233.
[24] P.G. Silver, Seismic anisotropy beneath the continents: probing the depths of geology, Annu. Rev. Earth Planet. Sci. 24 (1996) 385–432.
[25] P.G. Silver, S.S. Gao, K.H. Liu, Kaapvaal Seismic Group, Mantle deformation beneath southern Africa, Geophys. Res. Lett. 28 (2001) 2493–2496.
[26] P.G. Silver, M. Fouch, S. Gao, M. Schmitz, Seismic anisotropy, mantle fabric, and the magmatic evolution of Precambrian Southern Africa, S. Afr. J. Geol. (2004) (in press).
[27] C.J. Wolfe, P.G. Silver, Seismic anisotropy of oceanic upper mantle: shear wave splitting methodologies and observations, J. Geophys. Res. 103 (1998) 749–771.
[28] D.L. Schutt, E.D. Humpreys, P and S wave velocity and V_p/V_s in the wake of the Yellowstone hot spot, J. Geophys. Res. 109 (2004) (doi:10.1029/2003JB002442).
[29] G. Barruol, W.B. Ismaïl, Upper mantle anisotropy beneath the African IRIS and Geoscope stations, Geophys. J. Int. 146 (2001) 549–561.
[30] G. Helffrich, D.A. Wiens, E. Vera, S. Barrientos, P. Shore, S. Robertson, R. Adaros, A teleseismic shear-wave splitting study to investigate mantle flow around South America and implications for plate-driving forces, Geophys. J. Int. 149 (2002) F1–F7.
[31] G. Barruol, R. Hoffmann, Upper mantle anisotropy beneath the Geoscope stations, J. Geophys. Res. 104 (1999) 10757–10773.
[32] D.K. Blackman, J.-M. Kendall, Seismic anisotropy in the upper mantle: 2. Predictions for current plate boundary flow models, Geochem. Geophys. Geosys. 3 (2002) (doi:10.1029/2001GC000247).
[33] F. Boudier, A. Nicolas, Nature of the Moho transition zone in the Oman ophiolite, J. Petrol. 36 (1995) 777–796.
[34] W.B. Ismaïl, D. Mainprice, An olivine fabric database: an overview of upper mantle fabrics and seismic anisotropy, Tectonophysics 296 (1998) 145–157.
[35] P.G. Silver, M.K. Savage, The interpretation of shear-wave splitting parameters in the presence of two anisotropic layers, Geophys. J. Int. 119 (1994) 949–963.
[36] G. Rümpker, P.G. Silver, Apparent shear-wave splitting parameters in the presence of vertically varying anisotropy, Geophys. J. Int. 135 (1998) 790–800.
[37] E. Kaminski, N.M. Ribe, A kinematic model for recrystallization and texture development in olivine polycrystals, Earth Planet. Sci. Lett. 189 (2001) 253–267.
[38] H. Jung, S. Karato, Water-induced fabric transitions in olivine, Science 293 (2001) 1460–1463.
[39] J.E. Dixon, L. Leist, C. Langmui, J.-G. Schilling, Recycled dehydrated lithosphere observed in plume-influenced mid-ocean-ridge basalt, Nature 420 (2002) 385–389.
[40] C. DeMets, R.G. Gordon, D.F. Argus, S. Stein, Effect of recent revisions to the geomagnetic reversal time scale on estimates of current plate motions, Geophys. Res. Lett. 21 (1994) 2191–2194.
[41] A.E. Gripp, R.G. Gordon, Current plate velocities relative to

the hotspots incorporating the NUVEL-1 global plate motion model, Geophys. Res. Lett. 17 (1990) 1109–1112.
[42] B.H. Hager, R.J. O'Connell, A simple global model of plate dynamics and mantle convection, J. Geophys. Res. 86 (1981) 4843–4867.
[43] B.H. Hager, R.W. Clayton, Constraints on the structure of mantle convection using seismic observations, flow models, and the geoid, in: W.R., Title Mantle Convection: Plate Tectonics and Global Dynamics Peltier (Eds.), The Fluid Mechanics of Astrophysics and Geophysics, vol. 4, Gordon & Breach, New York, NY, 1989, pp. 657–763.
[44] T.H. Jordan, The continental tectosphere, Rev. Geophys. 13 (1975) 1–12.
[45] D.E. James, M.J. Fouch, J.C. VanDecar, S. van der Lee, Kaapvaal Seismic Group, Tectospheric structure beneath southern Africa, Geophys. Res. Lett. 28 (2001) 2485–2488.
[46] S. Karato, B.B. Karki, Origin of lateral variation of seismic wave velocities and density in the deep mantle, J. Geophys. Res. 106 (2001) 21771–21783.
[47] C.P. Conrad, C. Lithgow-Bertelloni, How mantle slabs drive plate tectonics, Science 298 (2002) 207–209.
[48] F.F. Pollitz, I.S. Sacks, Viscosity structure beneath northeast Iceland, J. Geophys. Res. 101 (1996) 17771–17793.
[49] J.X. Mitrovica, Haskell [1935] revisited, J. Geophys. Res. 101 (1996) 555–569.
[50] M. Ishii, J. Tromp, Normal-mode and free-air gravity constraints on lateral variations in velocity and density of Earth's mantle, Science 285 (1999) 1231–1236.
[51] J. Resovsky, J. Trampert, Using probabilistic seismic tomography to test mantle velocity–density relationships, Earth Planet. Sci. Lett. 215 (2003) 121–134.
[52] C. Thoraval, M.A. Richards, The geoid constraint in global geodynamics: viscosity structure, mantle heterogeneity models and boundary conditions, Geophys. J. Int. 131 (1997) 1–8.
[53] Y. Ricard, M. Richards, C. Lithgow-Bertelloni, Y. Le Stunff, A geodynamic model of mantle density heterogeneity, J. Geophys. Res. 98 (1993) 21895–21909.
[54] C. Lithgow-Bertelloni, M.A. Richards, The dynamics of Cenozoic and Mesozoic plate motions, Rev. Geophys. 36 (1998) 27–78.
[55] A.A. Nyblade, S.W. Robinson, The African Superswell, Geophys. Res. Lett. 21 (1994) 765–768.
[56] F.G. Lemoine, et al., The Development of the Joint NASA GSFC and NIMA Geopotential Model EGM96, NASA/TP-1998-206861, 1998.
[57] A. Cazenave, Geoid, topography and distribution of landforms, in: T. Aherns (Ed.), Global Earth Physics, A Handbook of Physical Constants, AGU Reference Shelf, vol. 1, AGU, Washington, DC, 1995, pp. 32–39.